

## Article

# Simultaneous Action of X- and O-Mode HF Pump Waves on the High-Latitude Upper (F-Region) Ionosphere at EISCAT

Nataly Blagoveshchenskaya <sup>1,\*</sup> , Tatiana Borisova <sup>1</sup>, Alexey Kalishin <sup>1</sup>, Ivan Egorov <sup>1</sup>, Tim Yeoman <sup>2</sup> and Ingemar Haggstrom <sup>3</sup> 

<sup>1</sup> Department of Geophysics, Arctic and Antarctic Research Institute, 199397 St. Petersburg, Russia; borisova@aari.ru (T.B.); askalishin@aari.ru (A.K.); aaricoop@aari.ru (I.E.)

<sup>2</sup> School of Physics and Astronomy, University of Leicester, Leicester LE1 7RH, UK; yxo@leicester.ac.uk

<sup>3</sup> EISCAT Scientific Association, SE-961 28 Kiruna, Sweden; ingemar.haggstrom@eiscat.se

\* Correspondence: nataly@aari.ru

**Abstract:** We report experimental results from multi-instrument diagnostic tools related to phenomena in the high latitude ionosphere *F*-region, induced by the simultaneous action of powerful extraordinary (X-mode) and ordinary (O-mode) polarized HF radio waves at EISCAT (European Incoherent SCATter) during magnetically quiet background geophysical conditions. HF pump waves were injected towards the magnetic zenith at a frequency of 5.423 MHz, which was just below the critical frequency of the *F*<sub>2</sub> layer when the excitation of X- and O-mode phenomena was possible. In the course of the experiment, the effective radiated power (*ERP*) of the X-mode wave was 130.5 MW, while the portion of the O-mode *ERP* was 29.9 MW (about 20% of the full *ERP*). It was found that simultaneous action of the X- and O-mode pump waves lead to the excitation of effects typical for both X- and O-mode HF pump waves. Namely, the excitation of small-scale field-aligned irregularities due to the thermal parametric (resonance) instability and a downshifted maximum (DM) component in the wideband stimulated electromagnetic emission (WSEE) spectra, typical for the O-mode HF pumping, was observed, together with multiple ion gyro-harmonic structures in the narrowband stimulated electromagnetic emission (NSEE) spectra. These latter results were recorded at a large (more than 1000 km) distance from the EISCAT/heating facility, typical only for an X-mode HF pumping. The results obtained are compared with “pure” O-mode heating and discussed in detail.

**Keywords:** powerful HF radio wave; high latitude ionosphere; nonlinear process; instability; plasma waves; stimulated electromagnetic emission; field-aligned irregularities; EISCAT



**Citation:** Blagoveshchenskaya, N.; Borisova, T.; Kalishin, A.; Egorov, I.; Yeoman, T.; Haggstrom, I. Simultaneous Action of X- and O-Mode HF Pump Waves on the High-Latitude Upper (F-Region) Ionosphere at EISCAT. *Universe* **2022**, *8*, 91. <https://doi.org/10.3390/universe8020091>

Academic Editors: Anna Milillo and Vladislav Demyanov

Received: 27 December 2021

Accepted: 27 January 2022

Published: 29 January 2022

**Publisher's Note:** MDPI stays neutral with regard to jurisdictional claims in published maps and institutional affiliations.



**Copyright:** © 2022 by the authors. Licensee MDPI, Basel, Switzerland. This article is an open access article distributed under the terms and conditions of the Creative Commons Attribution (CC BY) license (<https://creativecommons.org/licenses/by/4.0/>).

## 1. Introduction

The investigation of the interaction between powerful high frequency (HF) radio waves (HF pump waves) and ionosphere plasma is an actively developing problem in the physics of ionospheric plasmas. Conducting physical experiments in the natural, free plasma of the ionosphere is of particular interest. Over the last five decades, considerable efforts have been undertaken into the investigation of phenomena in the upper (*F*-region) ionosphere induced by HF pump waves by using ground-based HF transmitters with high effective radiated power, so-called HF heating facilities. This provides the controlled investigations to explore in detail the nonlinear processes in the plasma, the excitation of turbulences and plasma waves, and the plasma and cyclotron resonances. HF pump waves with ordinary (O-mode) polarization are commonly used for the modification of the ionospheric *F*-region at all HF heating facilities in the world. The O-mode HF pump wave interacts with the ionospheric plasma most efficiently at the reflection altitude ( $f_H^2 = f_{po}^2$ , where  $f_H$  is the pump frequency and  $f_{po}$  is the local plasma frequency) and the upper hybrid resonance altitude ( $f_{UH}^2 = f_H^2 - f_{ce}^2$ , where  $f_{ce}$  is the electron gyro-frequency), giving rise to the excitation of parametric decay and thermal parametric (resonance) instabilities [1–4].

Such an interaction produces a large variety of phenomena in the ionospheric plasma. The most important among them are artificial field-aligned irregularities (FAIs) [5–9], stimulated electromagnetic emission (SEE) [10–13], HF-induced electron heating [9], artificial optical emission [8,9,14,15], anomalous absorption [16,17], and Langmuir and ion-acoustic plasma waves (see, for example, [3,4,8,18,19] and references therein).

The extraordinary polarized (X-mode) HF pump wave in the undisturbed background ionosphere is reflected at the altitude where the local plasma frequency is determined as  $f_{px}^2 = f_H (f_H - f_{ce})$ . That is, below the height of the existing electrostatic plasma waves (the Langmuir and upper hybrid ones). As a result, X-mode HF pump waves should not generate such waves and, as a consequence, the excitation of the artificial plasma turbulence and phenomena accompanying them. However, a large number of X-mode experiments, performed by the Russian team at EISCAT, clearly demonstrated for the first time that the X-polarized HF pump waves, injected into the high latitude ionospheric *F*-region towards the magnetic zenith, are able to produce the excitation of a large variety of HF-induced phenomena, which can even be much stronger than the O-mode effects [20–31].

While phenomena induced by O-mode HF pump waves are only generated at frequencies below the critical frequency of the ionospheric *F2* layer ( $f_H \leq f_oF2$ ), the X-mode phenomena are excited at pump frequencies lying below and above the critical frequency of the *F2* layer ( $f_H \leq f_oF2$  and  $f_H > f_oF2$ ) [25]. It is important that at  $f_H > f_oF2$ , the X-mode HF-induced plasma and ion lines (HFPLs and HFILs) in the EISCAT (930 MHz) radar spectra, which are signatures of the Langmuir and ion-acoustic plasma waves, occurred in the frequency range between the ordinary  $f_oF2$  and extraordinary  $f_xF2$  modes of the critical frequencies ( $f_oF2 \leq f_H \leq f_xF2$ ) and disappeared when  $f_H > f_xF2$  when the X-mode pump wave can no longer be reflected from the ionosphere [25]. Note that the relation between  $f_oF2$  and  $f_xF2$  is defined as  $f_xF2 = f_oF2 + f_{ce}/2$ , where  $f_{ce}$  is the electron gyro-frequency. However, the artificial small-scale field-aligned irregularities (FAIs) and narrowband stimulated electromagnetic emission (NSEE) continue to be generated when  $f_H > f_xF2$  and HFPLs and HFILs were no longer excited. In such a case, they were observed when the pump frequency exceeded  $f_xF2$  by up to 1.5 MHz [20,24,25,30,31].

Therefore, in the course of the X-mode HF pumping at frequencies above  $f_oF2$ , the “pure” X-mode phenomena are only generated, owing to the O-mode phenomena not being able to be excited because the pump wave is not reflected from the ionosphere. However, during X-mode heating at  $f_H \leq f_oF2$ , O-mode leakage effects cannot be completely excluded.

This article provides further insight into unresolved issues concerning the O-mode leakage effects. The main attention is paid to the analysis of experimental results from multi-instrument diagnostics obtained in the course of a specially designed EISCAT experiment. In this experiment, the EISCAT/heating facility radiated simultaneously, in a controlled way, both X-mode and O-mode pump waves into the high latitude ionospheric *F*-region towards the magnetic zenith. We analyze the behavior and features of artificial field-aligned irregularities (FAIs), wideband and narrowband stimulated electromagnetic emissions (WSEE and NSEE), plasma parameters (electron density and temperature), and HF enhanced ion and plasma lines (HFIL, HFPL) and compare them with “pure” O-mode effects.

## 2. Experiment and Instrumentation

The EISCATHF heating experiment reported here was carried out by the Russian team on 28 October 2015 using the HF heating facility located near Tromsø, Norway (69.6° N, 19.2° E, magnetic dip angle  $I = 77^\circ$ ) [32]. HF pumping was produced in the field-aligned direction (the magnetic zenith) at frequency  $f_H = 5.423$  MHz using the high gain Array 1, with a beam width  $\sim 5\text{--}6^\circ$  at the  $-3$  dB level. The experiment was conducted under quiet magnetic conditions in the evening hours from 15:30 to 16 UT with the transmission scheme of 10 min on, 5 min off. The pump frequency was just below the critical frequency of the *F2*

layer ( $f_oF2$ ) and the fourth electron gyro harmonic ( $4f_{ce}$ ). In such conditions, the generation of both O- and X-mode phenomena is possible.

Figure 1 presents the calculated effective radiated power (ERP) and beam patterns in the course of the experiment on 28 October 2015. From 15:31 to 15:41 UT, the O-mode was radiated. The effective radiated power (ERP) was 362.4 MW during the first 6 min of the pump pulse (15:31–15:37 UT) and then reduced to 236.9 MW from 15:37 to 15:41 UT (see Figure 1a,b). The X-mode leakage was very low, about 0.6–0.7 MW. Therefore, almost “pure” O-mode HF pumping was produced in this pulse. In the next pump pulse from 15:46 to 15:56 UT, the simultaneous radiation of 29.9 MW (20% of full ERP) with the O-mode pump wave and 130.5 MW (80% of full ERP) with the X-mode wave was made (see Figure 1c).

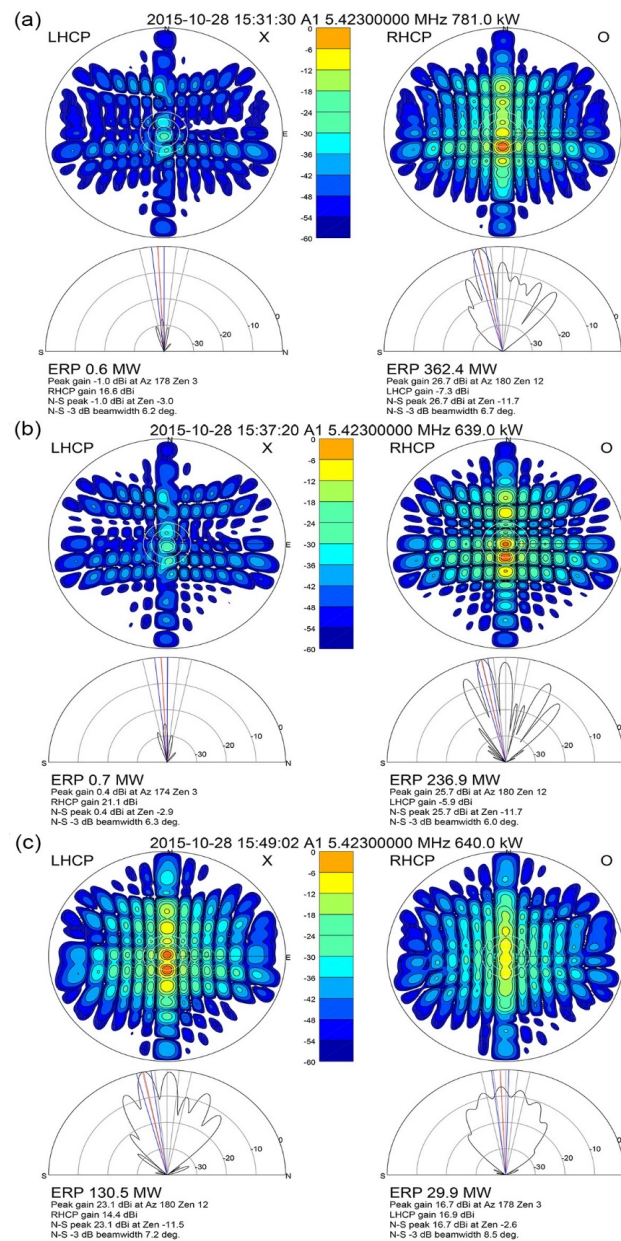


**Figure 1.** Calculated effective radiated power (ERP) and beam patterns of the extraordinary (X) and ordinary (O) HF pump waves on 28 October 2015 at (a) 15:31:30 UT, (b) 15:37:20 UT, and (c) 15:49:20 UT (calculations have been performed by M.T. Rietveld).

Multi-instrument diagnostics were utilized for the investigation of various phenomena induced by the simultaneous action of the O- and X-mode pump waves and their comparison with “pure” O-mode effects. Wideband stimulated electromagnetic emission (WSEE) measurements were carried out in a frequency band of 200 kHz about 12 km away from the EISCAT/heating. Details of the WSEE receiver can be found in [33]. Observations of narrowband stimulated electromagnetic emission (NSEE), within  $\pm 1$  kHz of the pump frequency, were performed near St. Petersburg ( $60.27^\circ$  N,  $29.37^\circ$  E) at a distance of 1200 km, far away from the EISCAT/Heating facility. Signals from the HF heater were processed by a digital spectrum analyzer, the ICOM-R75 receiver, with a 90 dB dynamic range, a frequency resolution of 0.4 Hz, and a temporal resolution of 2.4 s. The CUTLASS (Co-operative UK Twin Located Auroral Sounding System) radar [34] at Hankasalmi, Finland ( $62.3^\circ$  N;  $26.6^\circ$  E) was utilized for the diagnostic of artificial small-scale field-aligned irregularities (FAIs). The CUTLASS radar operated at six frequencies within 10 and 20 MHz on a single beam directed over Tromsø with a range gate of 15 km and a temporal resolution of 3 s. The EISCAT UHF incoherent scatter radar (933 MHz) [35] co-located with the EISCAT/heating facility ran in the same direction as the HF heater (field-aligned). It provides the plasma parameters and Langmuir and ion-acoustic plasma waves seen in the radar spectra as the HF-enhanced plasma and ion lines. The UHF radar data were processed with the Grand Unified Incoherent Scatter Design and Analysis Package [36]. The reliability of the plasma parameters used in the analysis was checked by the value of the Residual parameter  $R \leq 2$  [36].

### 3. Results and Analysis

#### 3.1. Behavior and Features of the Stimulated Electromagnetic Emission and Small-Scale Artificial Field-Aligned Irregularities

Stimulated electromagnetic emission (SEE) was observed for the first time by Thidé et al. [10] at the HF heater near Tromsø. During the next four decades, the various spectral components in the frequency band  $\pm 100$  kHz from the pump frequency were extensively investigated at all HF heating facilities in the world (see, for example, [11,37] and references therein). The downshifted maximum (DM) is a commonly occurring spectral feature in the wideband stimulated electromagnetic emission (WSEE) spectrum, observed in the close vicinity of HF heating facilities under O-mode HF pumping at frequencies below the critical frequency  $f_oF2$  and away from the electron gyro-harmonics. The DM peak intensity is typically observed at  $\Delta f_- = \Delta f_{DM} \approx 2 \times 10^{-3} f_H$  [11].

Figure 2 demonstrates the spectrograms of the stimulated electromagnetic emissions (wideband in the frequency band  $\pm 100$  kHz and narrowband in the frequency band  $\pm 1$  kHz of the heater frequency) observed on 28 October 2015 from 15:30 to 16:00 UT. As seen from Figure 2a, the spectrogram of the wideband stimulated electromagnetic emission (WSEE) obtained near Tromsø exhibits a spectral component, downshifted from the pump frequency  $f_H = 5.423$  MHz by about  $\Delta f_- = 11$  kHz, observed in the pump pulses from 15:31 to 15:41 UT (almost pure O-mode HF pumping) and from 15:46 to 15:56 UT (simultaneous action of the X- and O-mode HF pump waves). Note that in a large number of our previous X-mode experiments with a small leakage of the O-mode wave ( $ERP \leq 5$  MW), the DM component was never observed [21,25]. It is unexpected that in the course of “pure” O-mode heating from the “cold start” with high  $ERP \approx 362$  MW, a weak DM component is generated, but its intensity increased when the  $ERP$  dropped to 237 MW. In the next pump pulse, when only 30 MW was radiated with the O-mode, an intense DM component occurred through the whole pump cycle. The effect of anomalous absorption is strongest when the O-mode pump frequency matches the  $f_oF2$  [17]. It was concluded [18] that anomalous absorption and self-absorption of the O-mode wave are stronger under high  $ERP$ . In such conditions, one would expect to observe a lower DM intensity under high  $ERP \approx 362$  MW as compared with cases of  $ERP \approx 237$  and 30 MW. Moreover, preconditioning may also produce the DM intensity enhancements in the second

part of the pump pulse from 15:31 to 15:41 UT. The DM excitation is closely related to the FAI generation [11].

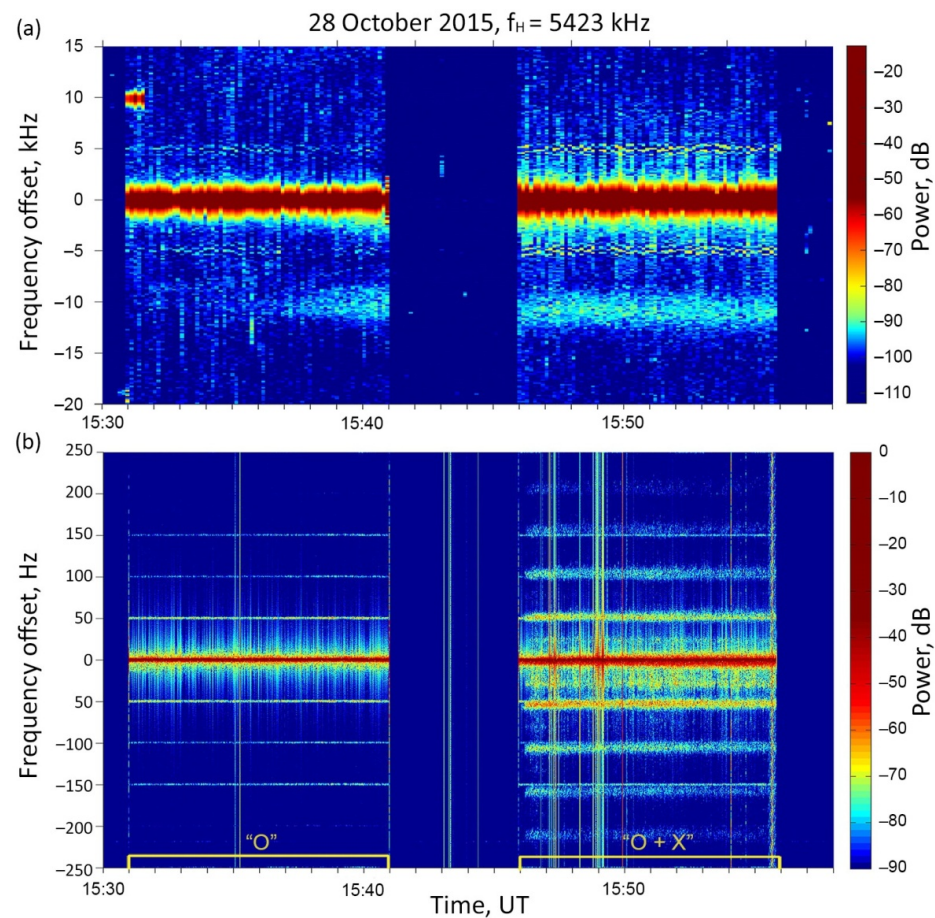


**Figure 2.** The spectrogram of (a) the wideband stimulated electromagnetic emission (WSEE) recorded in the close vicinity of the EISCAT/heating facility and (b) narrowband stimulated electromagnetic emission (NSEE) was observed at a distance of 1200 km from the heating facility in the course of the experiment on 28 October 2015 at a pump frequency  $f_H = 5.423$  MHz. The almost “pure” O-mode wave was radiated with effective radiated power of 362.4 MW from 15:31 to 15:37 UT and then reduced to 236.9 MW from 15:37 to 15:41 UT. The simultaneous radiation of 29.9 MW (20% of full ERP) with the O-mode pump wave and 130.5 MW (80% of full ERP) with the X-mode wave was made from 15:46 to 15:56 UT. The pump pulses and polarization of the heater wave are shown on the time axis.

The other feature, seen in the WSEE spectra observed in the close vicinity of the HF heating facility, is the occurrence of two symmetrical components shifted from the pump frequency by approximately  $\pm 5$  kHz. Wang et al. [33] attributed this feature to the novel component in the WSEE spectra excited by the X-mode HF pump wave. However, the same steady symmetrical component, but less pronounced, was also observed under “pure” O-mode heating from 15:31 to 15:41 UT (see Figure 2a). Actually, we cannot exclude a technical origin of the approximately  $\pm 5$  kHz component in the WSEE spectra observed under both O- and X-mode pump pulses.

The narrowband stimulated electromagnetic emission (NSEE) in the frequency band  $\pm 1$  kHz of the heater frequency, observed under O-mode HF pumping in the neighborhood of HF heaters, was recently found at the HAARP facility [12,13,38,39] and then at the EISCAT/heating facility [40,41]. The features and excitation mechanisms of various discrete structures in the NSEE spectrum were extensively investigated (see, for example, [13,41–44]). Our X-mode HF pumping experiments at EISCAT made it possible to

observe for the first time the NSEE at a large distance from the EISCAT/heating facility [25–27]. Alternating O/X-mode pumping has demonstrated clearly that only X-mode heating is able to produce NSEE observed far away from EISCAT.

Below we consider in detail the features of the narrowband stimulated electromagnetic emission (NSEE) in the frequency band  $\pm 1$  kHz of the pump frequency recorded at a distance of 1200 km away from the heating facility (see Figure 2b). It is evident that only during simultaneous radiation of the X- mode ( $ERP = 130.5$  MW) and O-mode pump wave ( $ERP = 29.9$  MW) from 16:46 to 16:56 UT that the NSEE spectra exhibit multiple down- and upshifted spectral components with respect to  $f_H$ , ordered by the ion gyro-frequency  $f_{ci}$  for  $O^+$  ions. In addition to the  $nf_{ci}$  spectral structures, the downshifted spectral component at  $0.5f_{ci}$  can be seen on the spectrogram. Similar multiple ion gyro-harmonic structures in the NSEE spectra were observed in our other X-mode experiments at different heater frequencies [25–27]. The observed structures in the NSEE spectra did not occur under “pure” O-mode HF pumping from 15:31 to 15:41 UT. Here, only the weak and narrow 50 Hz harmonics of the power supply can be seen on the spectrogram.

Let us consider in more detail the features and behavior of the multiple down- and upshifted ion gyro-harmonic structures in the NSEE spectra recorded far away from the EISCAT/heating facility. Figure 3 demonstrates the behavior of the intensities of upshifted and downshifted ion gyro-harmonic structures (Figure 3a,b respectively) in the course of a pump pulse from 15:46 to 15:56 UT. There is an asymmetry in the features of the NSEE upshifted and downshifted spectral components. As the harmonic number increases from the first to the fifth, the intensity of upshifted structures drops from  $-70$  dB to  $-91$  dB and the frequency offset increases from  $+52$  Hz to  $+255$  Hz, while the intensity of the downshifted structures drops from  $-63$  dB to  $-88$  dB and the frequency offset relative to the pump frequency changes from  $-56$  Hz to  $-265$  Hz, (see Figures 2 and 3). As was shown by Blagoveshchenskaya et al. [26] from an X-mode frequency stepping experiment through the fifth electron gyro-harmonic, the similar paired downshifted and upshifted spectral lines were strongest at pump frequencies below  $5f_{ce}$  and disappeared when the heater frequency  $f_H$  reached  $5f_{ce}$ .

Figure 4 shows the behavior in time of spectral widths for every upshifted and downshifted and ion gyro-harmonic structure (Figure 4a,b respectively) in the course of the pump pulse from 15:46 to 15:56 UT. The spectral width of every discrete structure was determined as the frequency band containing 50% of spectral power. It is clearly seen that increasing the harmonic number from the first to the fifth leads to a rise of spectral width from 6 to 17 Hz.

The power of downshifted spectral structures averaged through the pump cycle from 15:46 to 15:56 UT, and the delay in the time of occurrence of the spectral structures depending on the harmonic number is shown in Figure 5. With the rise of the harmonic number, the intensities of the discrete spectral components dropped and their delay in the time of occurrence, relative to the pump onset, increased. These features and behavior of the discrete spectral components indicate the presence of a cascade process in their excitation.

Kalishin et al. [27] proposed two relevant mechanisms responsible for the excitation of multiple discrete spectral structures induced by the X-mode HF pumping and observed at a large distance from the EISCAT/heating facility. The first is magnetized stimulated Brillouin scatter (MSBS) when an X-mode electromagnetic wave decays into a backscattered electromagnetic wave and an electrostatic ion gyro-harmonic mode. The second one is related to stimulated ion Bernstein scatter (SIBS), in which an X-mode HF pump wave decays into a high-frequency electron Bernstein wave and a low-frequency ion Bernstein wave. Multiple decays can be realized in both mechanisms, which leads to the development of a cascading process in the ion gyro-harmonic excitation. FAIs, generated in the artificially disturbed ionospheric patch, have a dominant role in NSEE observations far away from the EISCAT/heating facility [27].

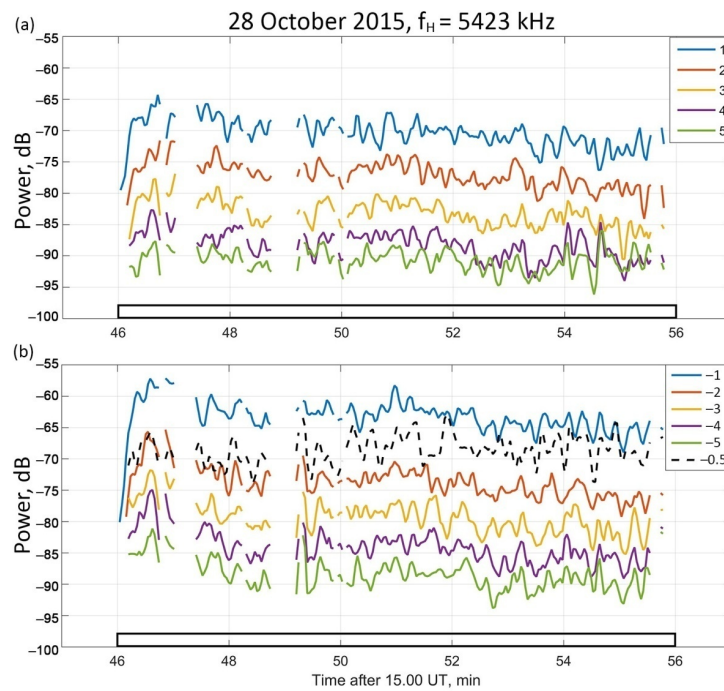


**Figure 3.** Behavior of intensities for (a) the upshifted from the first to the fifth (labeled as 1, 2, 3, 4, 5 and (b) downshifted ion gyro-harmonic structures (labeled as -1, -2, -3, -4, -5 and -0.5) in the course of pump pulse from 15:46 to 15:56 UT. Gaps in the intensities of the ion gyro-harmonic structures correspond to the presence of interference.

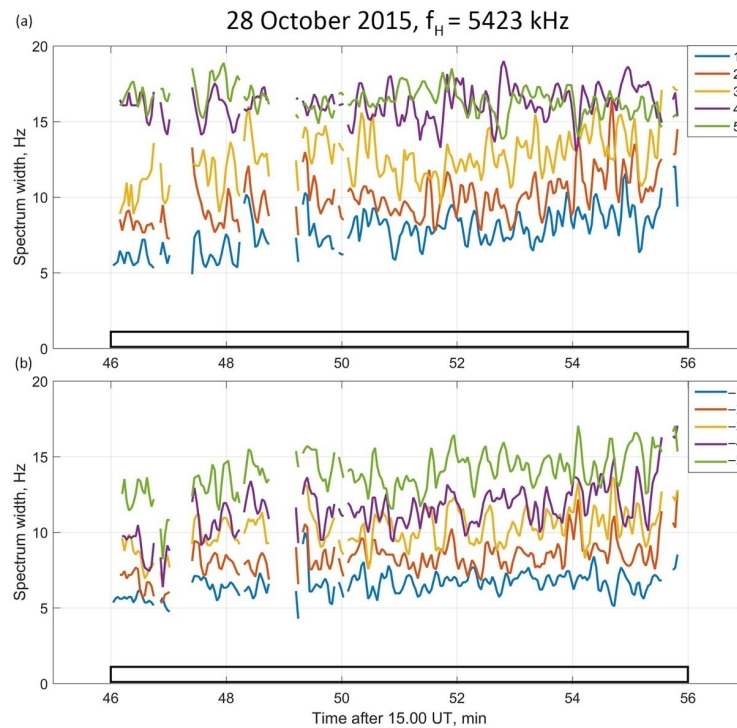


**Figure 4.** Behavior of spectral width for (a) the upshifted from the first to the fifth (labeled as 1, 2, 3, 4, 5 and (b) downshifted ion gyro-harmonic structures (labeled as -1, -2, -3, -4, -5 and -0.5) in the course of the pump pulse from 15:46 to 15:56 UT. Gaps in the spectral width of the ion gyro-harmonic structures correspond to the presence of interference.

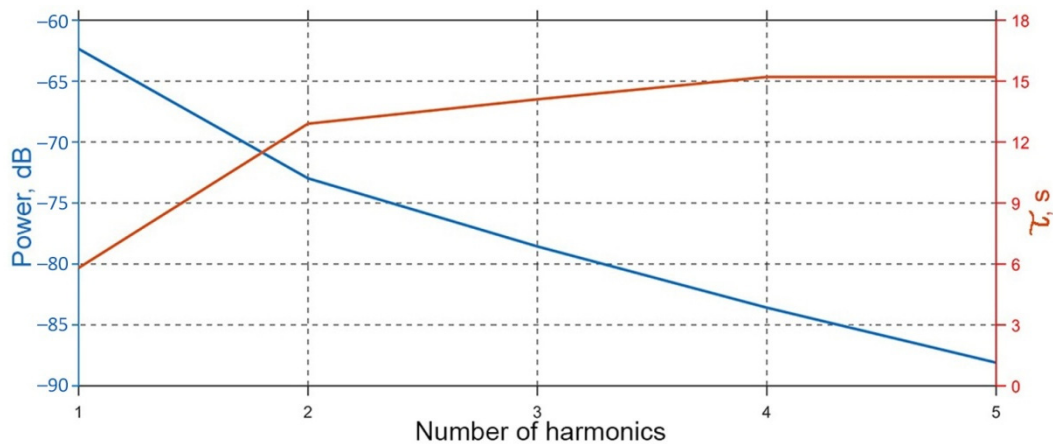


**Figure 5.** The power of downshifted spectral structures, averaged through the pump cycle, from 15:46 to 15:56 UT, and the delay in time of occurrence the spectral structures depending on the harmonic number.

The excitation of the DM component in the WSEE spectra and multiple ion gyro-harmonic structures in the NSEE spectra were accompanied by the generation of FAIs from the CUTLASS observations (see Figure 6). As seen from Figure 6, the signals backscattered from FAIs occurred at the CUTLASS operational frequencies about  $f_{\text{CUTLASS}} \approx 10, 11.5, 13.2, 16.3,$  and  $18$  MHz, owing to the Bragg condition corresponding to the FAI spatial size across the magnetic field  $l_{\perp} = 15, 13, 11.4, 9.2,$  and  $8.3$  m ( $l_{\perp} = c/2f_{\text{CUTLASS}}$ , where  $c$  is a speed of light). FAIs, with the spatial size within  $l_{\perp} = 8.3\text{--}11.4$  m, are the most intense in the course of the experiment. FAIs exhibit features, such as the growth and decay times, typical for O-mode heating in both pump pulses from 15:31 to 15:41 and 15:46 to 15:56 UT. The behavior and features of FAIs are very similar in both pump cycles. They appeared a few seconds after the EISCAT/heating was turned on and greatly decayed after it was turned off. These growth and decay times are typical for the O-mode FAIs [6–9].

### 3.2. Plasma Parameter Changes

The EISCAT UHF radar, co-located with the EISCAT/heating facility, is able to provide detailed investigations of the ionospheric plasma parameters (the electron density  $N_e$  and temperature  $T_e$ , and the ion temperature  $T_i$  and velocity  $V_i$ ) and Langmuir and ion-acoustic plasma waves. The latter was seen in the radar spectra as HF-enhanced plasma and ion lines (HFPLs and HFILs). Figure 7 demonstrates the overview of the EISCAT UHF radar observations on 28 October 2015 from 15:30 to 16:00 UT obtained with 20s integration time. This shows the altitude-temporal behavior of the electron density (Figure 7a) and temperature (Figure 7b) and the UHF radar backscatter, labeled as the raw electron density (Figure 7c). The increased UHF radar backscatter corresponds to the ion line enhancements. The electron density and temperature at fixed heights depending on the time are depicted in Figure 8a,b, respectively.

Under “pure” O-mode HF pumping with high  $ERP \approx 362$  MW from 15:31 to 15:37 UT strong thermal  $T_e$  enhancements up to 200% above the background level are detected in a wide altitude range. At 15:37 UT, the  $ERP$  was reduced to  $\sim 236$  MW leading to a  $T_e$  fall.

The raw electron density behavior clearly demonstrates that the O-mode HF pumping onset is accompanied by abrupt ion line enhancements followed by a descending altitude. The UHF radar backscatter power, labeled in Figure 7c as the raw electron density, is a manifestation of HF-enhanced ion lines. Similar altitude-descending HF-enhanced ion layers under an O-mode HF pumping were observed and investigated from a large number of heating experiments [19,22,45–47]. After an initial overshoot, the re-appearance of enhanced ion lines, coexisting with intense FAIs, occurred. However, the  $ERP$  reduced at 15:37 UT caused the disappearance of persistent ion lines (Figure 7c), which re-appeared only at the end of the pump pulse.

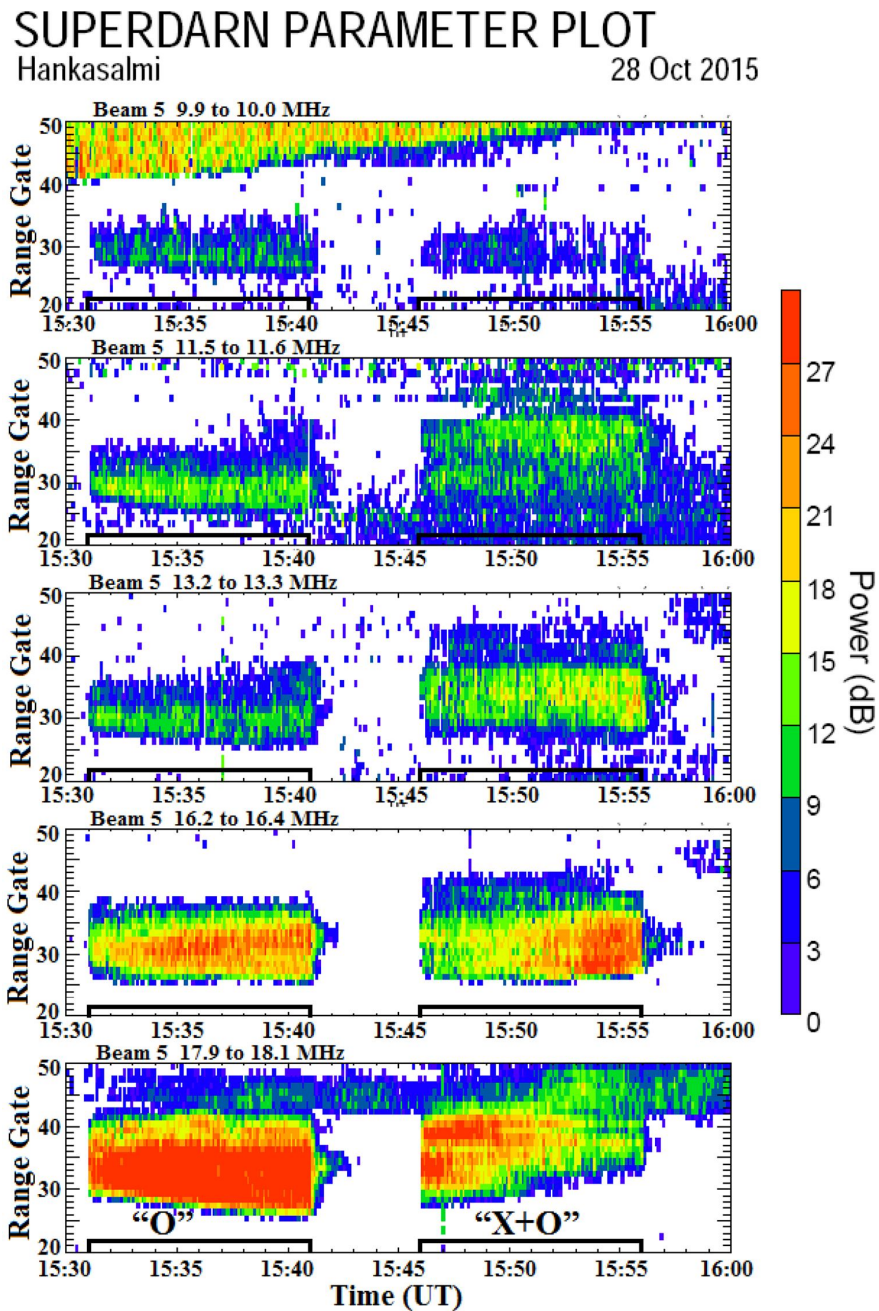


**Figure 6.** The backscatter power from CUTLASS Hankasalmi (Finland) radar observations (beam 5) at operational frequencies about of 10, 11.5, 13.2, 16, 18 MHz in range gate—time coordinates on 28 October 2015 from 15:30 to 16:00 UT. The distance from Hankasalmi to the heated ionospheric path over Tromsø corresponds to range gates 30–35.

The radiation of the O-mode pump wave with  $ERP \approx 30$  MW (20%) and the X-mode wave with  $ERP \approx 130$  MW (80% of full  $ERP$ ) was mixed in the transmission pulse from 15:46 to 15:56 UT. The heating effects are seen in the  $T_e$  enhancements, which are induced both the thermal (by an O-mode wave) and ohmic (by an X-mode wave) heating. As was shown by Bryers et al. [38], for O-mode heating, the height-integrated heating rate due to the thermal heating mechanism is higher than the theoretical ohmic electron heating rate by 2–5 times. Some weak  $N_e$  enhancements induced by an X-mode pump wave are detected from 15:46 to 15:56 UT. These  $N_e$  enhancements occurred at altitudes well above the  $T_e$  enhancements (see Figure 8). Note that in a large number of our previous X-mode experiments [21–23,25,31], strong  $N_e$  enhancements in a wide altitude range were also

observed at altitudes over the  $T_e$  enhancements, whether the HF-enhanced ion and plasma lines were excited or not.

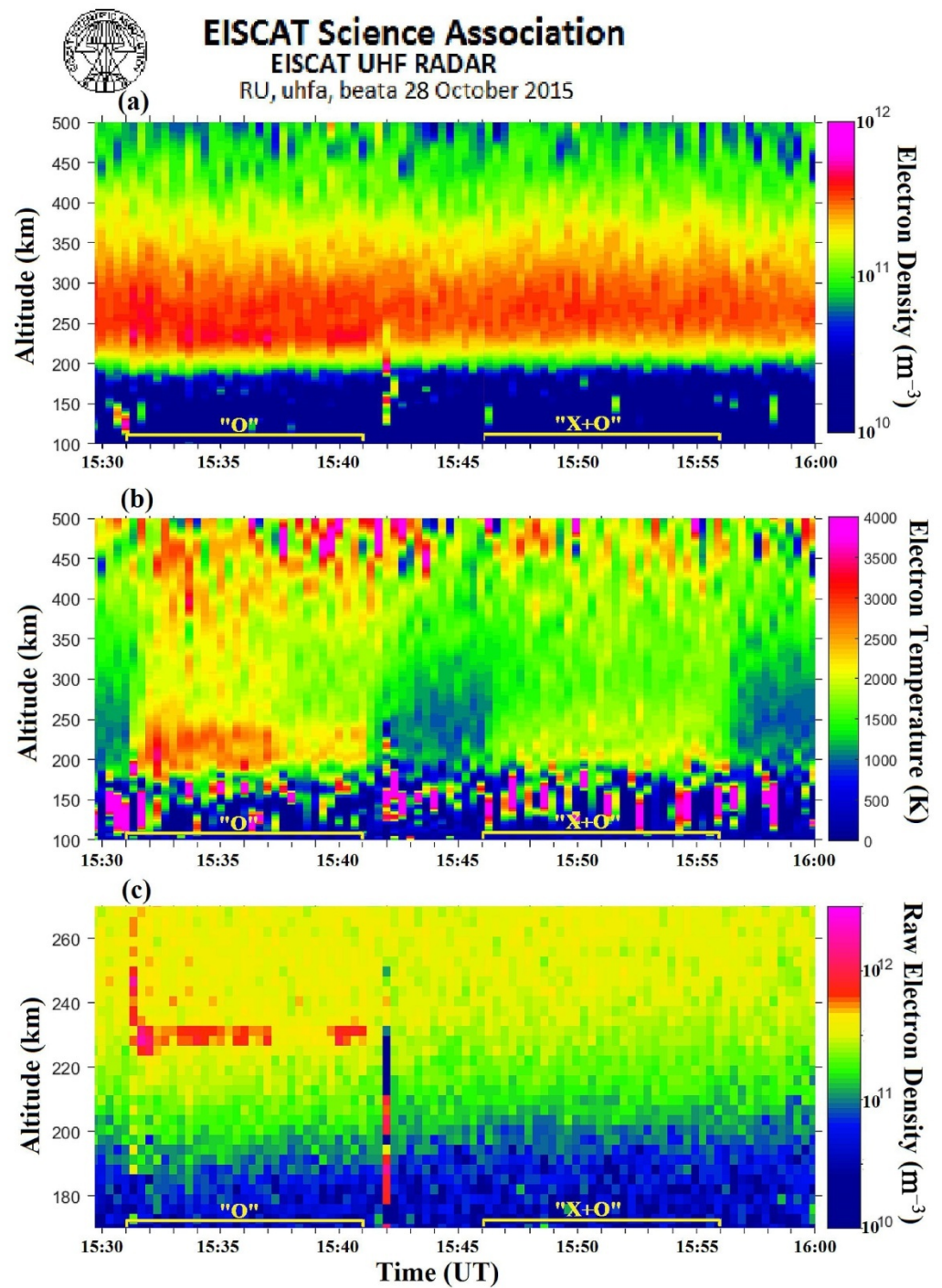


**Figure 7.** EISCAT UHF radar observations with 20 s integration time on 28 October 2015 from 15:30 to 16:00 UT of (a) electron density, (b) electron temperature, and (c) raw electron density. The pump pulses and polarization of the heater wave are shown on the time axis.

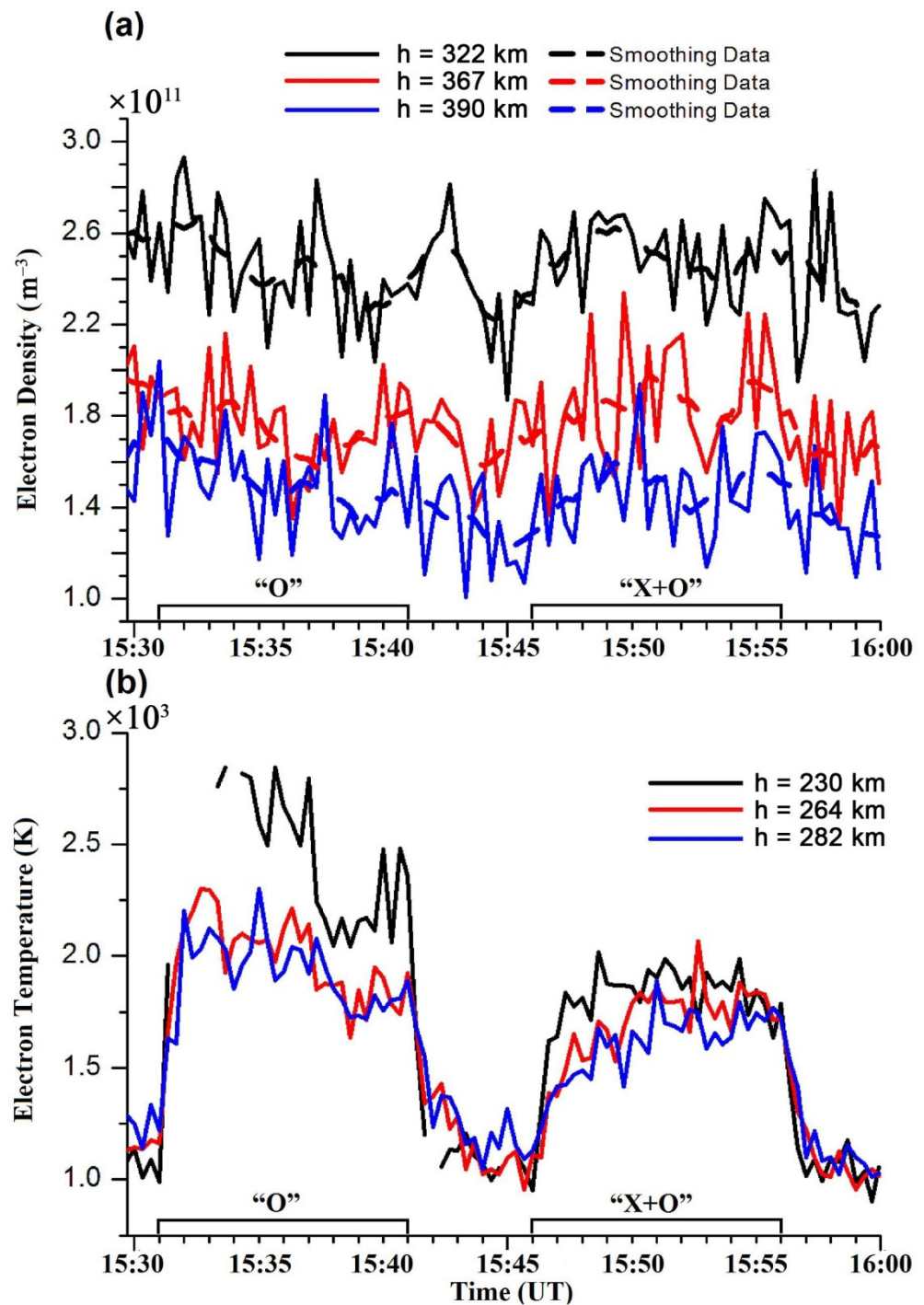


**Figure 8.** The temporal behavior of (a) the electron density and (b) electron temperature at fixed heights from the EISCAT radar observations on 28 October 2015 from 15:30 to 16:00 UT. The pump pulses and polarization of the pump wave are shown on the time axis.

### 3.3. Langmuir and Ion-Acoustic Plasma Waves

EISCAT UHF radar provides direct measurements of Langmuir and ion-acoustic plasma waves seen in the radar spectra as HF-enhanced plasma and ion lines. Figure 9 shows the intensities of the HF-induced downshifted and upshifted ion lines (HFIL<sub>DOWN</sub> and HFIL<sub>UP</sub>), plasma lines (HFPL), and outshifted plasma lines (HFPL<sub>OUT</sub>) at fixed heights in the course of the experiment on 28 October 2015 from 15:30 to 16 UT. Both the EISCAT UHF radar and HF heating facility run in the magnetic field-aligned direction. Figures 10 and 11 demonstrate spectra of HFIL and HFPL, respectively, taken with 5 s

resolution for a fixed time in the course of the O-mode HF pump pulse from 15:31 to 15:41 UT at the altitudes with their maximum intensities. Note that incoherent scatter radars detect Langmuir and ion-acoustic plasma waves as coherent backscatter, leading to the enhanced ion-line spectra. As a consequence, at altitudes occupied by ion and plasma lines, the electron temperature and density cannot be correctly estimated [36].

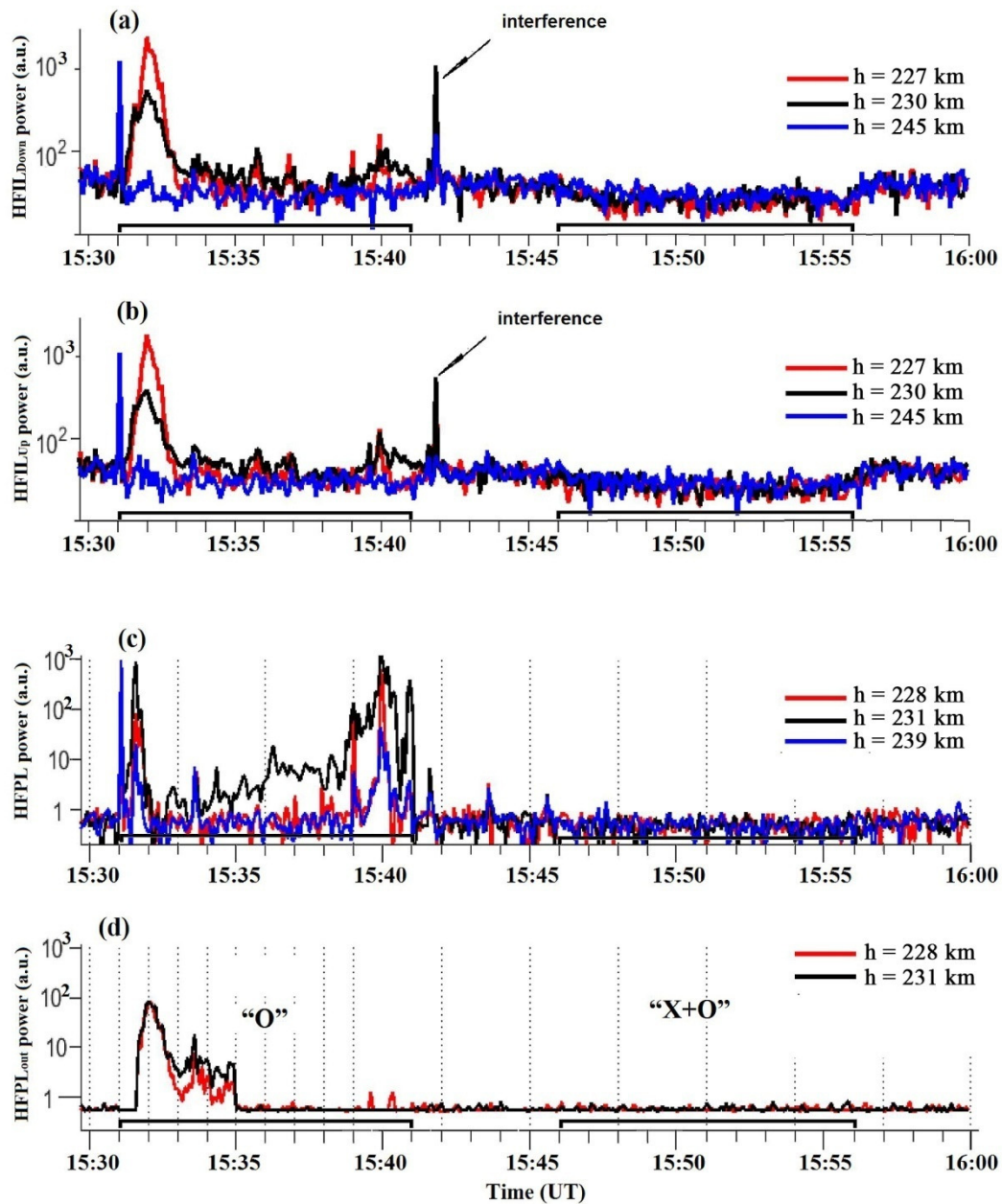


**Figure 9.** Temporal behavior of (a) the HF-induced downshifted ion lines, (b) upshifted ion lines, (c) downshifted plasma lines, and (d) outshifted plasma lines at fixed heights in the course of the experiment on 28 October 2015 from 15:30 to 16 UT. Data were obtained with a 5 s integration time. The pump pulses and polarization of the pump wave are shown on the time axis.

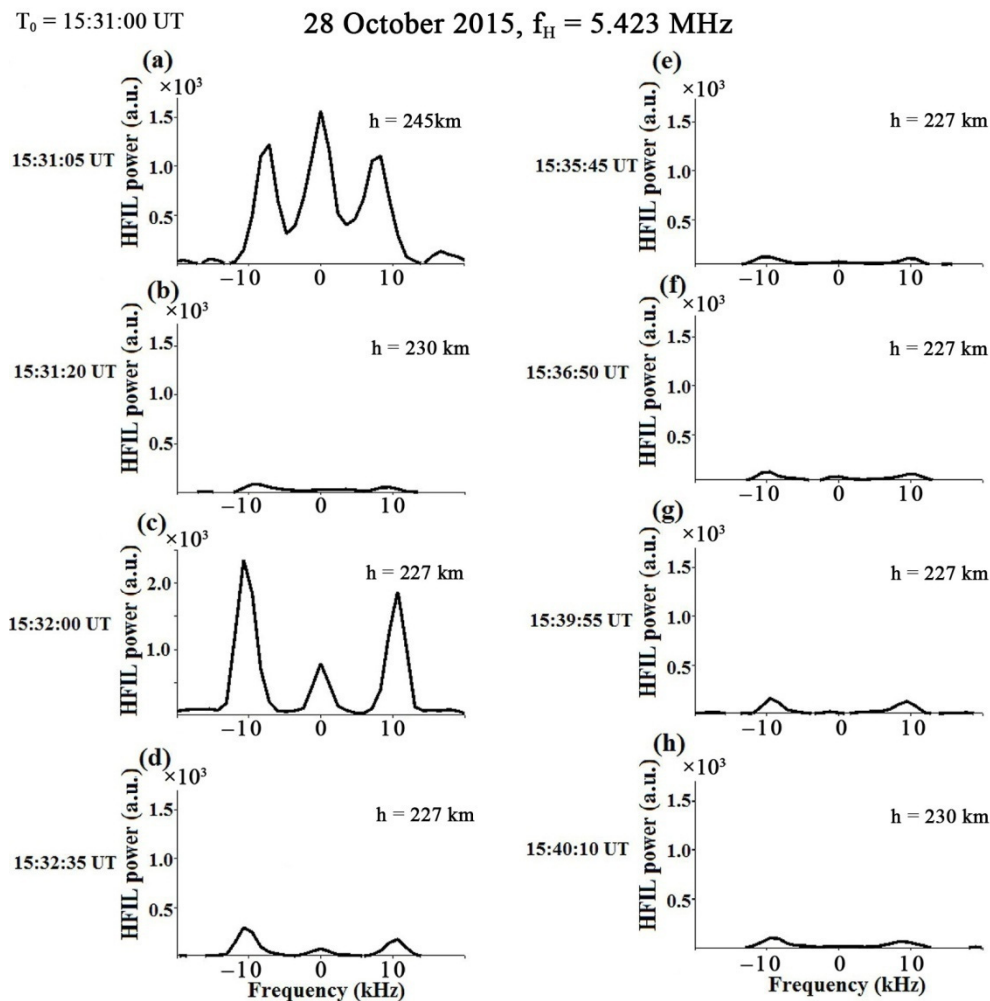


**Figure 10.** Spectra of HF-induced ion lines taken with 5 s resolution at the altitudes of their maximum intensities during the “pure” O-mode pulse from 15:31 to 15:41 UT at (a) 15:31:05 UT, (b) 15:31:20 UT, (c) 15:32:00 UT, (d) 15:32:35 UT, (e) 15:35:45 UT, (f) 15:36:50 UT, (g) 15: 39:55 UT, (h) 15:40:00 UT.

As seen, during “pure” O-mode HF pumping from 15:31 to 15:41 UT, the HF-enhanced ion and plasma lines are observed in the first 5 s radar dump (known as the initial overshoot), which is an indication of the generation of the “classic” parametric decay instability (PDI), when the pump electromagnetic waves decay into the Langmuir and ion-acoustic plasma waves [3,4,18]. It acts as an immediate response to the onset of HF pumping (the initial overshoot) and could be observed by the EISCAT UHF radar during an O-mode HF pumping with an ERP above 21–43 MW [18]. The overshoot effect is pronounced in the first few seconds after the heating onset and then diminishes in intensity on time scales corresponding to the FAI growth of a few seconds giving rise to the anomalous absorption of the pump wave energy [48]. Moreover, the spectra of ion and plasma lines (see Figures 10 and 11) exhibit the “zero” component that is a typical feature of the oscillating two-stream instability (OTSI). For the OTSI excitation a higher effective radiated power is required as compared with the “classic” PDI [4,18,49]. The small-scale artificial field-aligned irregularities (FAIs) cause the anomalous absorption, acting to diminish the pump wave power below the threshold needed for the PDI and OTSI excitation and limit the further generation of HFIL and HFPL [16,48].

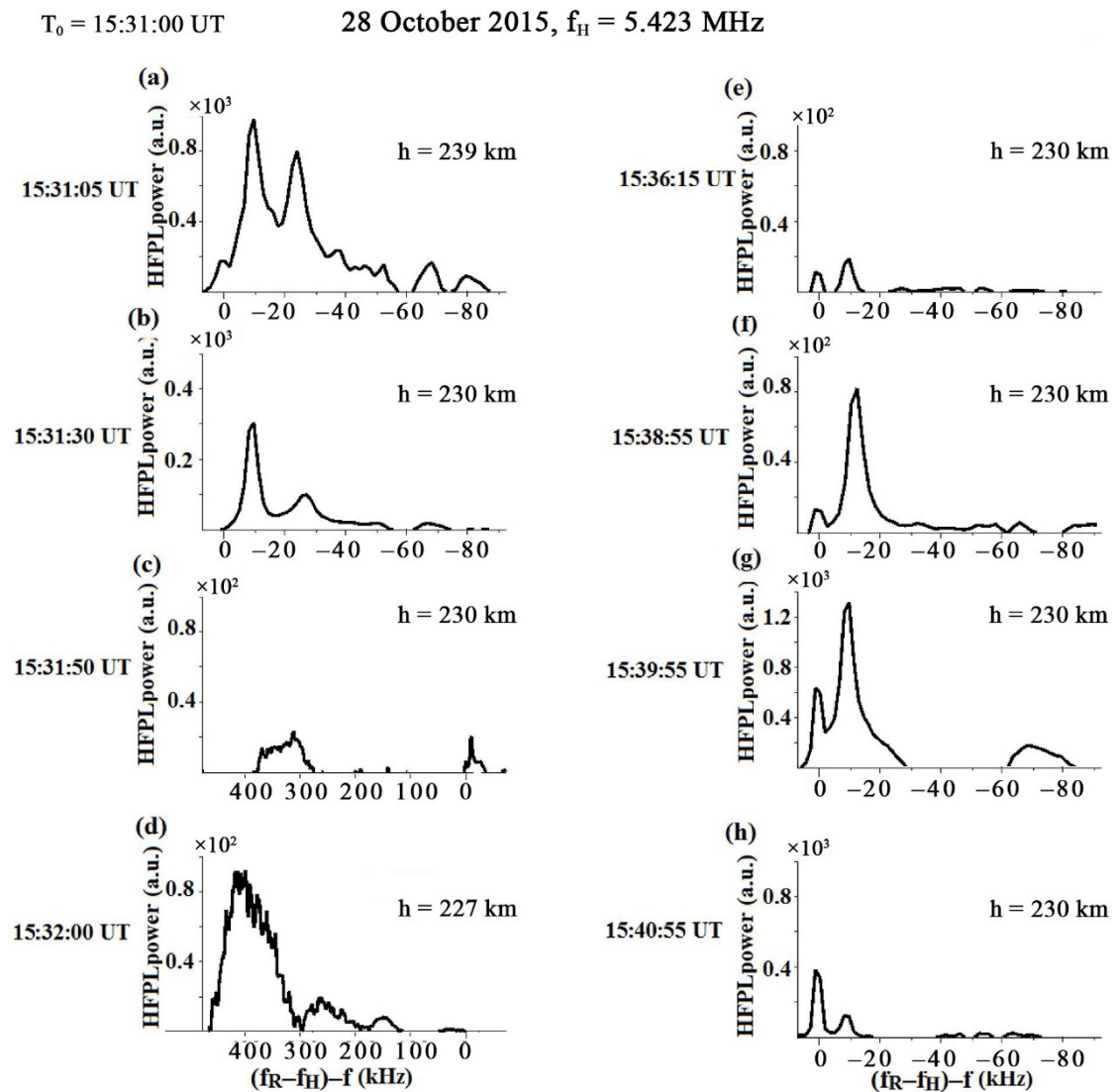


**Figure 11.** Spectra of HF-induced plasma lines taken with 5 s resolution at the altitudes of their maximum intensities during the “pure” O-mode pulse from 15:31 to 15:41 UT at (a) 15:31:05 UT, (b) 15:31:30 UT, (c) 15:31:50 UT, (d) 15:32:00 UT, (e) 15:36:15 UT, (f) 15:36:55 UT, (g) 15:39:55 UT, (h) 15:40:55 UT.

However, under high effective radiated power ( $ERP > 150\text{--}200$  MW), the re-appearance of HFIL and HFPL can occur [23]. The re-appearance of persistent HFIL and HFPL, coexisting with intense FAIs, occurred in the course of “pure” O-mode HF pumping with  $ERP \approx 362$  MW (see Figures 9–11). In addition, the outshifted plasma line was also excited (see Figures 9 and 11). Recall that the experiment on 28 October 2015 was carried out at the pump frequency close to the critical frequency of the F2 layer and just below the fourth electron gyro-harmonic. In the same conditions, the outshifted plasma lines were excited during other O-mode pumping experiments at EISCAT. This plasma line, shifted by 0.30–0.45 MHz relative to the heater frequency, is the so-called free mode [50–52]. As time progresses, the spectral power of HFPLs, HFILs, and outshifted plasma lines diminish. However, towards the end of the O-mode pump pulse, the HFPLs and weak HFILs are detected again.

In the course of mixed radiation of  $\sim 30$  MW with the O-mode and  $\sim 130$  MW with the X-mode from 15:46 to 15:56 UT, neither HFILs nor HFPLs were excited at all (see Figure 9). This means that the 30 MW O-mode pump power is not able even to excite the “classic” PDI as an immediate response to the HF pumping onset. The more so as the excitation

of persistent O-mode ion and plasma lines is not possible owing to that requiring much higher pump power as compared with the initial overshoot [23,28]. On the other side, the X-mode heater power flux of 130 MW is deficient for the excitation of persistent Langmuir and ion-acoustic plasma waves that require  $ERP \geq 150\text{--}200$  MW [23].

#### 4. Discussion

A specially designed EISCAT experiment was conducted under quiet magnetic conditions at pump frequency  $f_H = 5.423$  MHz lying very close to the critical frequency  $f_oF2 \approx 5.5$  MHz and just below the fourth electron gyro-harmonic  $4f_{ce} = 5.44$  MHz. In this experiment, the EISCAT/heating facility radiated simultaneously in a controlled way for both the X-mode and O-mode pump waves. The O-mode pump wave with  $ERP \approx 30$  MW (20% of the full ERP) and the X-mode wave with  $ERP \approx 130$  MW (80% of full ERP) were radiated into the high latitude ionospheric F-region towards the magnetic zenith. It is important that the sufficiently low X-mode heater power of  $\sim 130$  MW was chosen to exclude the excitation of the X-mode HF-induced plasma and ion lines. The results obtained were compared with “pure” O-mode HF pumping effects.

Experimental results, obtained under simultaneous radiation with both X- and O-mode HF pump waves from 15:46 to 15:56 UT, clearly demonstrate that phenomena typical for both X- and O-mode pumping were generated. The generation of various phenomena induced by simultaneous action of O- and X-mode HF pump waves is governed by the effective radiated power of O- and X-mode waves and thresholds required for the excitation of one kind or another phenomenon. One of the prominent phenomena, typical only for X-mode HF pumping, is the generation of the narrowband stimulated electromagnetic emission (NSEE) in the frequency band of  $\pm 1$  kHz relative to  $f_H$ , recorded at a large distance (about 1200 km) from the EISCAT/Heating facility. However, the FAIs and DM components in the WSEE spectra were induced by the O-mode pump power of 30 MW. HF-induced plasma and ion lines were not excited at all under mixed O- and X-mode HF pumping.

Let us estimate the excitation thresholds of the thermal parametric (resonance) instability (TPI), the parametric decay (PDI), the oscillating two-stream instabilities (OTSI), and the non-resonant decay instability (NRM) for the conditions of this experiment.

The threshold electric field of the O-mode HF pump wave, required for the excitation of the thermal parametric (resonance) instability (TPI), responsible for the FAI excitation, is given in the form [1,16,49]:

$$E_{TPI}^2 = 2.44 \frac{T_{e0}^2 (2\pi f_H)^2 k_B^2 k \cos \varphi}{p \nu_e 2\pi f_{ce} e^2 H} e^{-2\nu_e H/c}. \tag{1}$$

Here,  $T_{e0}$  is the unperturbed electron temperature,  $f_H$  is the pump wave frequency,  $f_{ce}$  is the electron gyro-frequency,  $k_B$  is the Boltzmann constant,  $k$  is the FAI wave number,  $\varphi$  is the angle between the local vertical and the magnetic field direction,  $\nu_e = \nu_{en} + \nu_{ei}$  is the electron collision frequency,  $\nu_{en}$  is the electron-neutral collision frequency,  $\nu_{ei}$  is the electron–ion collision frequency,  $c$  is a speed of light,  $H$  is the plasma scale height given by  $H = k_B(T_e + T_i)/gm_i$ , where  $T_e$  and  $T_i$  are the electron and ion temperatures, respectively,  $g$  is the acceleration due to gravity, and  $m_i$  is the ion mass,  $p$  is the ratio between the reflected and radiated powers of the pump wave; it can be assumed that  $p \approx 1$  within the first few seconds of the heating cycle.

The threshold electric field of the O-mode HF pump wave required for the excitation of parametric decay instability (PDI) in the ionosphere, assuming that the electric field of the pump wave is parallel to the Earth’s magnetic field at altitudes close to the reflection height, is given by expression [16,49,53] in the form:

$$E_{PDI}^2 = 4 \frac{N_{e0} k_B T_i \nu_e}{2\pi f_p \epsilon_0 B_{\max}}. \tag{2}$$

The threshold electric field of the O-mode pump wave for an oscillating two-stream instability (OTSI) is defined in [49,54] as

$$E_{\text{OTSI}}^2 = 4 \frac{T_e + T_i}{T_i} \frac{N_{e0} k_B T_i v_e}{2\pi f_p \epsilon_0}. \tag{3}$$

Here,  $N_{e0}$  is the electron density,  $f_p$  is the local plasma frequency at the reflection altitude of the heater wave,  $f_p^2 = f_H^2$ ,  $\epsilon_0$  is the dielectric constant, and the  $B_{\text{max}}$  is a function of the ratio  $T_e/T_i$ .

The expressions (1)–(3) allow us to estimate the  $E_{\text{TPI}}$ ,  $E_{\text{PDI}}$ , and  $E_{\text{OTSI}}$  by using values of the electron density and the electron and ion temperatures from the EISCAT UHF radar measurements within 15:30–16:00 UT and putting  $B_{\text{max}} = 0.56$  for  $T_e/T_i = 2$  [54]. The neutral and collisions are obtained from NRLMSISE-00 [55] as follows: the electron-neutral collision frequencies  $\nu_{en} = 5.4 \times 10^{-10} N_n T_e^{1/2}$ , where  $N_n$  is the neutral particle density, and the electron–ion collision frequencies  $\nu_{ei} = (34 + 4.18 \cdot \lg T_e^2 / N_e) \cdot N_e \cdot T_e^{-3/2}$ .

For the conditions of the experiment on 28 October 2015, the thresholds of electric field for the O-mode pump wave, required for the excitation of the thermal parametric instability (TPI), the parametric decay instability (PDI), and the oscillating two-stream instability (OTSI) were obtained as follows:  $E_{\text{TPI}} \approx 0.08$  V/m,  $E_{\text{PDI}} \approx 0.21$  V/m, and  $E_{\text{OTSI}} \approx 0.26$  V/m. The PDI and OTSI act as an immediate response to the onset of HF pumping (the initial overshoot). Then the development of small-scale artificial field-aligned irregularities (FAIs) causes the anomalous absorption and prevents further generation of the PDI and OTSI [16,48]. However, under high effective radiated power ( $ERP > 150\text{--}200$  MW), the re-appearance of persistent HF-enhanced ion and plasma lines coexisting with FAIs can occur. Certainly, this process requires a higher  $ERP$  as compared with the  $ERP$  required for the excitation of “classic” PDI and OTSI.

The threshold electric field of the O-mode pump wave, required for the excitation of the non-resonant decay instability (NRM), following the immediate excitation of PDI and OTSI is given in the form [3]:

$$E_{\text{NRM}} = \left( \frac{m_e m_i}{e^2} \cdot \frac{k_1 C_s \omega_{k\theta}^3 v_e v_i}{2\omega_{pe}^2 (k_{\parallel}^2 + k_{\perp}^2 \omega_{k\theta}^2 / (\omega_{k\theta}^2 - \Omega_e^2))} \right) \cdot \left[ 1 + \frac{16k_1^2 C_s^2}{v_e (v_e + 2v_i)} \right] \cdot \left[ \frac{v_e}{v_e + 2v_i} \right]^{1/2} \tag{4}$$

Here,  $k_1$  is the wave vector of the Langmuir wave excited by the pump wave as a result of the primary (electromagnetic) process of the parametric decay instability,  $k_{\parallel} = k_1 \cos \theta$ ,  $k_{\perp} = k_1 \sin \theta$ ,  $\theta$  is the inclination angle of the magnetic field;  $\omega_{k\theta}^2 = \omega_p^2 + 3k_B^2 V_{te}^2 + \Omega_e^2 \sin^2 \theta$ , where  $\omega_{pe} = (4\pi N_e e^2 / m_e)^{1/2}$ ,  $V_{te} = \sqrt{k_B T_e / m_e}$ ,  $\Omega_e = 2\pi f_{ce}$  are the plasma frequency, the thermal velocity, and the angular electron gyro-frequency, respectively;  $v_e$  and  $v_i$  are the electron and ion collision frequencies;  $\nu_i = \nu_{in} + \nu_{iL}$ ,  $\nu_{iL} = \sqrt{\pi/2} \omega_{IA}^{3/2} \sqrt{T_e/T_i} \exp[-(3 + T_e/T_i)/2]$  correspond to the ion Landau damping;  $\omega_{IA} = C_s k_{IA}$  is the angular frequency of the ion-acoustic wave and  $C_s = \sqrt{(T_e + 3T_i)/m_i}$  is the velocity of the ion-acoustic wave.

From expression (4), with allowance for the parameter values  $k_1 = 38.23 \text{ m}^{-1}$ ,  $k_{\perp} = 8.13 \text{ m}^{-1}$  (for the EISCAT radar at a frequency of 933 MHz),  $T_e = 1300$  K,  $T_i = 1000$  K,  $f_{ce} = 1.35$  MHz,  $C_s = 1330$  m/s,  $\nu_{iL} = 18.500$  kHz, the threshold of electric field of the O-mode pump wave, required for the excitation of Langmuir waves by the non-resonant mechanism, is  $E_{\text{NRM}} = 0.65$  V/m.

The effective radiated power in free space required for the excitation of TPI, PDI, OTSI, and NRM can be determined from the well-known expression [16]:

$$E[\text{V/m}] = \frac{0.25 \sqrt{ERP[\text{kW}]}}{h[\text{km}]}, \tag{5}$$

where  $h$  is the altitude of the disturbed ionospheric region above the Earth’s surface.

Then, for  $E_{\text{TPI}} \approx 0.08$  V/m,  $E_{\text{PDI}} \approx 0.21$  V/m,  $E_{\text{OTSI}} \approx 0.26$  V/m, and  $E_{\text{NRM}} = 0.65$  V/m, the effective radiated power thresholds can be obtained as follows:  $ERP_{\text{TPI}} = 8.5$  MW,  $ERP_{\text{PDI}} = 37.3$  MW,  $ERP_{\text{OTSI}} = 57.2$  MW, and  $ERP_{\text{NRM}} = 357.6$  MW.

As is evident, in the course of simultaneous action of the X- and O-mode HF pump waves from 15:46 to 15:56 UT, the FAIs could certainly be produced by the O-mode wave with  $ERP = 30$  MW due to the  $ERP_{TPI}$  being only 8.5 MW. The thresholds required for the excitation of the PDI and OTSI exceeded the O-mode radiated power of 30 MW, implying that these instabilities cannot be generated. At the same time, as seen from the EISCAT UHF radar measurements, the X-mode radiated power  $ERP \approx 130$  MW was not able to produce the persistent HFILs and HFPLs, coexisting with intense FAIs. The results from the EISCAT/Heating power stepping experiment demonstrated that the excitation threshold for the persistent HFILs and HFPLs, coexisting with FAIs, should exceed  $ERP > 150\text{--}200$  MW [23].

During almost “pure” O-mode heating with  $ERP \approx 360$  MW, strong PDI and OTSI, manifesting themselves as HFIL and HFPL from EISCAT UHF radar measurements, are excited as an immediate response to the HF pump onset (the initial overshoot). The EISCAT/heating effective radiated power is far in excess of  $ERP_{PDI} = 37.3$  MW and  $ERP_{OTSI} = 57.2$  MW. Thereafter the re-appearance of the HFILs and HFPL, coexisting with FAIs, occurred. We suggest that the non-resonant mechanism proposed in [3] with the excitation threshold  $ERP_{NRM} = 357.6$  MW could be responsible for that phenomenon. It should be noted that the O-mode radiated power was very close to  $ERP_{NRM}$ , resulting in the persistent ion and plasma lines coexisting with FAIs, exhibiting an unstable behavior. The enhancements of HFILs and HFPLs at the end of the 10 min CW pump pulse were possibly produced by the preconditioning effect.

The results from a specially designed EISCAT experiment, in which both X- and O-mode HF pump waves were radiated simultaneously in a controlled way, are important for correct analysis of possible O-mode leakage effects in the course of X-mode pumping experiments. Generally, the leakage of the O-mode wave does not exceed 5 MW ( $ERP \leq 5$  MW). As obvious from the results presented here, the 30 MW O-mode portion mixed in the 130 MW of X-mode was not able to excite the persistent HF-enhanced ion and plasma lines, coexisting with intense FAIs. As was shown, the excitation threshold of persistent HFILs and HFPLs requires much higher effective radiated power. Therefore, the small O-mode leakage certainly could not excite the persistent HF-enhanced ion and plasma lines, coexisting with FAIs, in the X-mode heating experiments at EISCAT.

## 5. Conclusions

We report the experimental results obtained in the course of the EISCAT specially designed experiment on 28 October 2015 carried out in the evening hours under quiet conditions. The EISCAT/heating facility radiated simultaneously, in a controlled way, both the X-mode and O-mode pump waves at the frequency of 5.423 MHz, lying just below the critical frequency  $f_oF2$  and the fourth electron gyro-harmonic. The O-mode pump wave with effective radiated power  $ERP \approx 30$  MW (20% of the full  $ERP$ ), mixed with the X-mode wave with  $ERP \approx 130$  MW (80% of full  $ERP$ ), were radiated into the high latitude ionospheric F-region towards the magnetic zenith. The sufficiently low X-mode heater power of 130 MW was chosen to exclude the excitation of the persistent X-mode HF-induced plasma and ion lines that have the excitation threshold  $ERP > 150\text{--}200$  MW [23].

It was found from multi-instrument diagnostics that phenomena typical for both X- and O-mode pumping were generated under simultaneous radiation with both X- and O-mode HF pump waves. The generation of various phenomena induced by simultaneous action of O- and X-mode HF pump waves is governed by the effective radiated power of O- and X-mode waves and thresholds required for the excitation of one kind or another phenomenon. Namely, the excitation of small-scale field-aligned irregularities (FAIs) due to the thermal parametric (resonance) instability and a downshifted maximum (DM) component in the wideband stimulated electromagnetic emission (WSEE) spectra, typical for the O-mode HF pumping, were observed together with the multiple ion gyro-harmonic structures in the narrowband stimulated electromagnetic emission (NSEE) spectra, recorded at a

large (more than 1000km) distance from the EISCAT/heating facility, typical only for an X-mode HF pumping. HF-induced plasma and ion lines were not excited at all.

It was shown that almost “pure” O-mode heating with  $ERP \approx 360$  MW produces the strong PDI and OTSI as an immediate response to the HF pump onset (the initial overshoot). Thereafter the re-appearance of the HFILs and HFPLs, coexisting with FAIs, was observed due to the non-resonant mechanism proposed in [3].

The article provides further insight into unresolved issues concerning the O-mode leakage during the X-mode experiments at EISCAT at pump frequencies below the critical frequency ( $f_H \leq f_oF2$ ). Generally, the leakage of the O-mode wave in the course of the X-mode HF pumping experiments does not exceed 5 MW ( $ERP \leq 5$  MW). The results presented here clearly demonstrate that the 30 MW O-mode portion mixed in the 130 MW of X-mode was not able to produce the persistent HFILs and HFPLs, coexisting with intense FAIs. Therefore, the small O-mode leakage certainly could not excite the persistent HF-enhanced ion and plasma lines in the X-mode heating experiments at EISCAT.

**Author Contributions:** Conceptualization, N.B.; methodology, N.B.; software, T.B., A.K., T.Y. and I.H.; investigation and analysis, N.B., T.B., A.K., I.E., T.Y. and I.H.; writing—original draft preparation, N.B.; writing—review and editing, N.B. and T.Y. All authors have read and agreed to the published version of the manuscript.

**Funding:** This research received no external funding.

**Institutional Review Board Statement:** Not applicable.

**Informed Consent Statement:** Not applicable.

**Data Availability Statement:** Data sets analyzed in this study were obtained in the course of our EISCAT heating experiment. The data can be obtained through the EISCAT Madrigal database (<https://portal.eiscat.se/madrigal/> (accessed on 26 December 2021)).

**Acknowledgments:** EISCAT is an international scientific association supported by research organizations in China (CRIRP), Finland (SA), Japan (NIPR and STEL), Norway (NFR), Sweden (VR), and the United Kingdom (NERC). The authors acknowledge the use of SuperDARN data. SuperDARN is a collection of radars funded by the national scientific funding agencies of Australia, Canada, China, France, Italy, Japan, Norway, South Africa, the United Kingdom, and the United States. The authors are thankful to M.T. Rietveld for the calculations of effective radiated powers and beam patterns under O- and X-mode HF pumping. T.Y. is supported by Science and Technology Facilities Council Grant ST/H002480/1.

**Conflicts of Interest:** The authors declare no conflict of interest.

## References

1. Grach, S.M.; Trakhtengerts, V.Y. Parametric excitation of ionospheric irregularities extended along the magnetic field. *Radiophys. Quant. Electron.* **1975**, *18*, 951–957. [CrossRef]
2. Gurevich, A.V. Nonlinear effects in the ionosphere. *Phys.-Uspekhi* **2007**, *50*, 1091–1121. [CrossRef]
3. Kuo, S.P. Overview of Ionospheric Modification by High Frequency (HF) Heaters-Theory. *Prog. Electromagn. Res. B* **2014**, *60*, 141–155. [CrossRef]
4. DuBois, D.F.; Rose, H.A.; Russell, D. Space and time distribution of HF excited Langmuir turbulence in the ionosphere: Comparison of theory and experiment. *J. Geophys. Res.* **1993**, *98*, 17543–17567. [CrossRef]
5. Minkoff, J.; Kugelman, P.; Weissman, I. Radio frequency scattering from a heated ionospheric volume, 1, VHF/UHF field-aligned and plasma-line backscatter measurements. *Radio Sci.* **1974**, *9*, 941–955. [CrossRef]
6. Bond, G.E.; Robinson, T.R.; Eglitis, P.; Wright, D.M.; Stocker, A.J.; Rietveld, M.T.; Jones, T.B. Spatial observations by the CUTLASS coherent scatter radar of ionospheric modification by high power radio waves. *Ann. Geophys.* **1997**, *15*, 1412–1421. [CrossRef]
7. Wright, D.M.; Davies, J.A.; Yeoman, T.K.; Robinson, T.R.; Shergill, H. Saturation and hysteresis effects in ionospheric modification experiments observed by the CUTLASS and EISCAT radars. *Ann. Geophys.* **2006**, *24*, 543–553. [CrossRef]
8. Streltsov, A.V.; Berthelier, J.-J.; Chernyshov, A.A.; Frolov, V.L.; Honary, F.; Kosch, M.J.; McCoy, R.P.; Mishin, E.V.; Rietveld, M.T. Past, Present and Future of Active Radio Frequency Experiments in Space. *Space Sci. Rev.* **2018**, *214*, 118. [CrossRef]
9. Rietveld, M.T.; Kosch, M.T.; Blagoveshchenskaya, N.F.; Kornienko, V.A.; Leyser, T.B.; Yeoman, T.M. Ionospheric electron heating, optical emissions, and striations induced by powerful HF radio waves at high latitudes: Aspect angle dependence. *J. Geophys. Res.* **2003**, *108*, 1141–1156. [CrossRef]

10. Thidé, B.; Kopka, H.; Stubbe, P. Observations of stimulated scattering of a strong high frequency radio wave in the ionosphere. *Phys. Rev. Lett.* **1982**, *49*, 1561–1564. [[CrossRef](#)]
11. Leyser, T.B. Stimulated electromagnetic emissions by high-frequency electromagnetic pumping of the ionospheric plasma. *Space Sci. Rev.* **2001**, *98*, 223–328. [[CrossRef](#)]
12. Norin, L.; Leyser, T.B.; Nordblad, E.; Thidé, B.; McCarrick, M. Unprecedentedly strong and narrow electromagnetic emissions stimulated by high-frequency radio waves in the ionosphere. *Phys. Rev. Lett.* **2009**, *102*, 065003. [[CrossRef](#)] [[PubMed](#)]
13. Bernhardt, P.A.; Selcher, C.A.; Kowtha, S. Electron and ion Bernstein waves excited in the ionosphere by high power EM waves at the second harmonic of the electron cyclotron frequency. *Geophys. Res. Lett.* **2011**, *38*, L19107. [[CrossRef](#)]
14. Brandstrom, B.U.E.; Leyser, T.B.; Steen, A.; Rietveld, M.T.; Gustavsson, B.; Aso, T.; Ejiri, M. Unambiguous evidence of HF pump-enhanced airglow. *Geophys. Res. Lett.* **1999**, *26*, 3561–3564. [[CrossRef](#)]
15. Pedersen, T.; Carlson, H. First observations of HF heater-produced airglow at the High Frequency Active Auroral Research Program facility: Thermal excitation and spatial structuring. *Radio Sci.* **2001**, *36*, 1013–1026. [[CrossRef](#)]
16. Robinson, T.R. The heating of the high latitude ionosphere by high power radio waves. *Phys. Rep.* **1989**, *179*, 79–209. [[CrossRef](#)]
17. Graham, K.N.; Fejer, J.A. Anomalous radio wave absorption due to ionospheric heating effects. *Radio Sci.* **1976**, *11*, 1057–1063. [[CrossRef](#)]
18. Stubbe, P.; Kohl, H.; Rietveld, M.T. Langmuir turbulence and ionospheric modification. *J. Geophys. Res.* **1992**, *97*, 6285–6297. [[CrossRef](#)]
19. Mishin, E.; Watkins, B.; Lehtinen, N.; Eliasson, B.; Pedersen, T.; Grach, S. Artificial ionospheric layers driven by high-frequency radiowaves: An assessment. *J. Geophys. Res. Space Phys.* **2016**, *121*, 3497–3524. [[CrossRef](#)]
20. Blagoveshchenskaya, N.F.; Borisova, T.D.; Yeoman, T.; Rietveld, M.T.; Ivanova, I.M.; Baddeley, L.J. Artificial field-aligned irregularities in the high-latitude F region of the ionosphere induced by an X-mode HF heater wave. *Geophys. Res. Lett.* **2011**, *38*, L08802. [[CrossRef](#)]
21. Blagoveshchenskaya, N.F.; Borisova, T.D.; Kosch, M.; Sergienko, T.; Brändström, U.; Yeoman, T.K.; Häggström, I. Optical and Ionospheric Phenomena at EISCAT under Continuous X-mode HF Pumping. *J. Geophys. Res. Space Phys.* **2014**, *119*, 10483–10498. [[CrossRef](#)]
22. Blagoveshchenskaya, N.F.; Borisova, T.D.; Yeoman, T.K. Comment on the article “Parametric Instability Induced by X-Mode Wave Heating at EISCAT” by Wang et al. 2016. *J. Geophys. Res. Space Phys.* **2017**, *122*, 12570–12586. [[CrossRef](#)]
23. Blagoveshchenskaya, N.F.; Borisova, T.D.; Kalishin, A.S.; Yeoman, T.K.; Häggström, I. Distinctive features of Langmuir and Ion-acoustic Turbulences induced by O- and X-mode HF Pumping at EISCAT. *J. Geophys. Res. Space Phys.* **2020**, *125*, e2020JA028203. [[CrossRef](#)]
24. Blagoveshchenskaya, N.F.; Borisova, T.D.; Yeoman, T.K.; Rietveld, M.T.; Häggström, I.; Ivanova, I.M. Plasma modifications induced by an X-mode HF heater wave in the high latitude F region of the ionosphere. *J. Atmos. Sol. Terr. Phys.* **2013**, *105–106*, 231–244. [[CrossRef](#)]
25. Blagoveshchenskaya, N.F.; Borisova, T.D.; Yeoman, T.K.; Häggström, I.; Kalishin, A.S. Modification of the high latitude ionosphere F region by X-mode powerful HF radio waves: Experimental results from multi-instrument diagnostics. *J. Atmos. Solar-Terr. Phys.* **2015**, *135*, 50–63. [[CrossRef](#)]
26. Blagoveshchenskaya, N.F.; Borisova, T.D.; Kalishin, A.S.; Yeoman, T.K.; Häggström, I. First observations of electron gyro-harmonic effects under X-mode HF pumping the high latitude ionospheric F-region. *J. Atmos. Solar-Terr. Phys.* **2017**, *155*, 36–49. [[CrossRef](#)]
27. Kalishin, A.S.; Blagoveshchenskaya, N.F.; Borisova, T.D.; Yeoman, T.K. Ion Gyro-Harmonic Structures in Stimulated Emission Excited by X-Mode High Power HF Radio Waves at EISCAT. *J. Geophys. Res. Space Phys.* **2021**, *126*, e2020JA028989. [[CrossRef](#)]
28. Borisova, T.D.; Blagoveshchenskaya, N.F.; Yeoman, T.K.; Häggström, I. Excitation of artificial turbulence in the high-latitude ionospheric F region as a function of the EISCAT/Heating effective radiated. *Radiophys. Quant. Electron.* **2017**, *60*, 273–290. [[CrossRef](#)]
29. Blagoveshchenskaya, N.F.; Borisova, T.D.; Kalishin, A.S.; Kayatkin, V.N.; Yeoman, T.K.; Häggström, I. Comparison of the Effects Induced by the Ordinary (O-Mode) and Extraordinary (X-Mode) Polarized Powerful HF Radio Waves in the High-Latitude Ionospheric F Region. *Cosm. Res.* **2018**, *56*, 11–25. [[CrossRef](#)]
30. Blagoveshchenskaya, N.F.; Borisova, T.D.; Kalishin, A.S.; Yeoman, T.K.; Schmelev, Y.A.; Leonenko, E.E. Characterization of Artificial, Small-Scale, Ionospheric Irregularities in the High-Latitude F Region Induced by High-Power, High-Frequency Radio Waves of Extraordinary Polarization. *Geomagn. Aeron.* **2019**, *59*, 759–773. [[CrossRef](#)]
31. Blagoveshchenskaya, N.F. Perturbing the high-latitude upper ionosphere (F region) with powerful HF radio waves: A 25-year collaboration with EISCAT. *URSI Radio Sci. Bull.* **2020**, *2020*, 40–55. [[CrossRef](#)]
32. Rietveld, M.T.; Senior, A.; Markkanen, J.; Westman, A. New capabilities of the upgraded EISCAT high-power HF facility. *Radio Sci.* **2016**, *51*, 1533–1546. [[CrossRef](#)]
33. Wang, X.; Zhou, C.; Xu, T.; Honary, F.; Rietveld, M.; Frolov, V. Stimulated electromagnetic emissions spectrum observed during an X-mode heating experiment at the European Incoherent Scatter Scientific Association. *Earth Planet. Phys.* **2019**, *3*, 391–399. [[CrossRef](#)]
34. Lester, M.; Chapman, P.J.; Cowley, S.W.H.; Crooks, S.J.; Davies, J.A.; Hamadyk, P.; McWilliams, K.A.; Milan, S.E.; Parsons, M.J.; Payne, D.B.; et al. Stereo CUTLASS: A new capability for the Super DARN radars. *Ann. Geophys.* **2004**, *22*, 459–473. [[CrossRef](#)]

35. Rishbeth, H.; Eyken, T. EISCAT: Early history and the first ten years of operation. *J. Atmos. Solar-Terr. Phys.* **1993**, *55*, 525–542. [[CrossRef](#)]
36. Lehtinen, M.S.; Huuskonen, A. General incoherent scatter analysis and GUIDAP. *J. Atmos. Solar-Terr. Phys.* **1996**, *58*, 435–452. [[CrossRef](#)]
37. Stubbe, P. Review of ionospheric modification experiments at Tromsø. *J. Atmos. Solar-Terr. Phys.* **1996**, *58*, 349–368. [[CrossRef](#)]
38. Bryers, C.J.; Kosch, M.J.; Senior, A.; Rietveld, M.T.; Singer, W. A comparison between resonant and nonresonant heating at EISCAT. *J. Geophys. Res. Space Phys.* **2013**, *118*, 6766–6776. [[CrossRef](#)]
39. Bernhardt, P.A.; Selcher, C.A.; Lehmberg, R.H.; Rodriguez, S.P.; Thomason, J.F.; Groves, K.M.; McCarrick, M.J.; Frazer, G.J. Stimulated Brillouin Scatter in a magnetized ionospheric plasma. *Phys. Rev. Lett.* **2010**, *104*, 165004. [[CrossRef](#)]
40. Borisova, T.D.; Blagoveshchenskaya, N.F.; Kalishin, A.S.; Kosch, M.; Senior, A.; Rietveld, M.T.; Yeoman, T.K.; Haggstrom, I. Phenomena in the high-latitude ionospheric F region induced by a HF heater wave at frequencies near the fourth electron gyroharmonic. *Radiophys. Quant. Electr.* **2014**, *57*, 1–19. [[CrossRef](#)]
41. Fu, H.Y.; Jiang, M.L.; Wang, K.N.; Wu, J.; Li, Q.L.; Rietveld, M.T.; Varberg, E.; Haggstrom, I.; Jin, Y.Q. Electron Temperature Inversion by Stimulated Brillouin Scattering During Electron Gyro-Harmonic Heating at EISCAT. *Geophys. Res. Lett.* **2020**, *47*, e2020GL089747. [[CrossRef](#)]
42. Mahmoudian, A.; Scales, W.A.; Bernhardt, P.A.; Fu, H.; Briczinski, S.J.; McCarrick, M.J. Investigation of ionospheric stimulated Brillouin scatter generated at pump frequencies near electron gyroharmonics. *Radio Sci.* **2013**, *48*, 685–697. [[CrossRef](#)]
43. Samimi, A.; Scales, W.A.; Fu, H.; Bernhardt, P.A.; Briczinski, S.J.; McCarrick, M.J. Ion gyroharmonic structures in stimulated radiation during second electron gyroharmonic heating: 1. Theory. *J. Geophys. Res. Space Phys.* **2013**, *118*, 502–514. [[CrossRef](#)]
44. Samimi, A.; Scales, W.A.; Bernhardt, P.A.; Briczinski, S.J.; McCarrick, M.J. Ion gyroharmonic structures in stimulated radiation during second electron gyroharmonic heating: 2. Simulations. *J. Geophys. Res. Space Phys.* **2014**, *119*, 462–478. [[CrossRef](#)]
45. Wu, J.; Blagoveshchenskaya, N.F.; Wu, J.; Rietveld, M.T.; Häggström, I. Descents in high-frequency enhanced plasma and ion lines during ionospheric heating at EISCAT. *J. Atmos. Solar-Terr. Phys.* **2021**, *212*, 105425. [[CrossRef](#)]
46. Ashrafi, M.; Kosch, M.; Honary, F. Heater-induced altitudedescent of the EISCAT UHF ion line enhancements: Observations and modeling. *Adv. Space Res.* **2006**, *38*, 2645–2652. [[CrossRef](#)]
47. Dhillon, R.S.; Robinson, T.R. Observations of time dependence and aspect sensitivity of regions of enhanced UHF backscatter associated with RF heating. *Ann. Geophys.* **2005**, *23*, 75–85. [[CrossRef](#)]
48. Jones, T.B.; Robinson, T.R.; Stubbe, P.; Kopka, H. EISCAT observations of the heated ionosphere. *J. Atmos. Solar-Terr. Phys.* **1986**, *48*, 1027–1035. [[CrossRef](#)]
49. Bryers, C.; Kosch, M.; Senior, A.; Rietveld, M.T.; Yeoman, T.K. The thresholds of ionospheric plasma instabilities pumped by high-frequency radio waves at EISCAT. *J. Geophys. Res. Space Phys.* **2013**, *118*, 7472–7481. [[CrossRef](#)]
50. Mishin, E.; Hagfors, T.; Kofman, W. On origin of outshifted plasma lines during HF modification experiments. *J. Geophys. Res.* **1997**, *102*, 27265–27269. [[CrossRef](#)]
51. Rietveld, M.T.; Isham, B.; Kohl, H.; Hoz, C.L.; Hagfors, T. Measurements of HF-enhanced plasma and ion lines at EISCAT with high altitude resolution. *J. Geophys. Res.* **2000**, *105*, 7429–7439. [[CrossRef](#)]
52. Borisova, T.D.; Blagoveshchenskaya, N.F.; Rietveld, M.T.; Häggström, I. Outshifted plasma lines observed in Heating experiments in the high-latitude ionosphere at pump frequencies near electron gyroharmonic. *Radiophys. Quant. Electr.* **2019**, *61*, 722–740. [[CrossRef](#)]
53. Fejer, J.A. Ionospheric Modification and Parametric Instabilities. *Rev. Geophys. Space Phys.* **1979**, *17*, 135–153. [[CrossRef](#)]
54. Stubbe, P.H.; Kopka, H. *Exploration of the Polar upper Atmosphere: Proceedings of the Nato Advanced Study Institute*; Deehr, C.S., Holtet, J.A., Eds.; Springer: Dordrecht, The Netherlands, 1981. [[CrossRef](#)]
55. Picone, J.M.; Hedin, A.E.; Drob, D.P.; Aikin, A.C. NRLMSISE-00 empirical model of the atmosphere: Statistical comparisons and scientific issues. *J. Geophys. Res.* **2002**, *107*, 1468. [[CrossRef](#)]